Surface characterization of nitrogen-doped Nb (100) large-grain superconducting RF cavity material

Arti Dangwal Pandey [1]*,

Guilherme Dalla Lana Semione [1,2],

Alena Prudnikava [1,2],

Thomas F. Keller [1,2],

Heshmat Noei [1],

Vedran Vonk [1]

Yegor Tamashevich[1,3]

Eckhard Elsen[1,4]

Brian Foster[1,2,5]

Andreas Stierle [1,2]

[1]*Deutsches Elektronen-Synchrotron (DESY), D-22607 Hamburg, Germany*

[2]*Fachbereich Physik, Universität Hamburg, D-22607 Hamburg, Germany*

[3]*Helmholtz-Zentrum Berlin für Materialien und Energie, D-14109 Berlin, Germany*

[4]*European Council for Nuclear Research (CERN), CH-1211 Geneva, Switzerland*

[5] *University of Oxford, Oxford, UK*

**Arti Dangwal Pandey: arti.pandey@desy.de*

Abstract

(100) oriented niobium (Nb) crystals annealed in the vacuum conditions close to that used in mass production of 1.3 GHz superconducting radio-frequency cavities for linear accelerators, and treated in nitrogen at a partial pressure of 0.04 mbar at temperatures of 800 °C and 900 °C have been studied. The surfaces of the nitrogen-treated samples were investigated by means of various surface-sensitive techniques, including grazing-incidence X-ray diffraction, X-ray photoemission spectroscopy and scanning electron microscopy with energy-dispersive X-ray spectroscopy in planar view and on cross-sections prepared by a focused ion beam. The appearance of a dense layer of epitaxial rectangular precipitates has been observed for the Niobium nitrided at 900°C. Increased nitrogen concentration in the near surface region was detected by glow-discharge optical-emission spectroscopy, focused ion-beam cross-sectional images and X-ray photoelectron spectroscopy. Crystalline phases of NbO and β-Nb_2N were identified by X-ray diffraction. This information was confirmed by X-ray photoelectron measurements, which in addition revealed the presence of Nb_2O_5, NbON, NbN and NbN_xO_y components on the surface. These results establish the near-surface Nb phase composition after high-temperature nitrogen treatment, which is important for obtaining a better understanding of the improved RF cavity performance.

Keywords

SRF cavities, niobium, niobium doping, surface characterization, XRD, XPS, electron microscopy

Introduction

Superconducting radio frequency (SRF) niobium cavities are widely used in x-ray free electron lasers, such as the European X-Ray Free-Electron Laser (EXFEL) as electron accelerating devices. Global efforts are being made to improve their performance in order to contribute to the realization of future international projects such as the International Linear Collider as well as the continuous wave operation of free electron lasers for providing very high luminosity, which becomes challenging due to several reasons, such as large facility power consumption and thermal load in the cold SRF cavities. The annealing of superconducting radio frequency niobium cavities in nitrogen atmospheres is known to result in the improvement of the quality factor (the ratio of the stored energy in the cavity to the power dissipation from the cavity walls in one RF period) by up to three times. However, the physico-chemical origin behind the success of the nitrogen treatment is still unclear.

Niobium is a transition metal with unique chemical, mechanical and physical properties. It possesses high corrosion resistance, large ductility, high strength at elevated temperatures, high melting point, low coefficient of linear thermal expansion, high thermal conductivity, and relatively low electrical resistivity. Apart from that, niobium is a type II superconductor and has the highest critical magnetic fields and critical temperature among pure elements. It is therefore widely used in modern accelerator technology employing SRF cavities to achieve high efficiency or quality factor and maximal accelerating fields. It is well established that the performance characteristics of such cavities are severely affected by thermal processing techniques upon which the impurity content (mainly hydrogen and oxygen) in the near-surface region, as well as the surface oxide structure, are modified [1, 2]. Recently, considerable progress has been made in the improvement of the quality factor of niobium cavities after a controlled annealing in a nitrogen atmosphere, which results in a decreased residual resistance [3, 4, 5]. The so called "nitrogen doping" procedure, which includes nitridation of 1.3 GHz fine-grain niobium cavities at 800 °C for a few minutes in 0.03-0.08 mbar of N_2 followed by electrochemical polishing (EP) that removes approximately 5 μm of material, was shown to demonstrate an extraordinarily high quality factor ($Q_0 \sim 5 \times 10^{10}$), exceeding that of pure niobium by several times [5, 6], while the N-treated cavities- prior to EP- performed poorly ($Q_0 \sim 10^7$). The performance characteristics of the nitrogen-treated cavities depend on the amount of material etched away from the cavity interior. Since 2013, the nitrogen treatment of cavities has been a topic of intense research, nevertheless only little data are available on the structural characterization of these surfaces [7, 8].

Typically, in most earlier reported work, the nitrogen diffusion is carried out at relatively high temperatures (1300-2000 °C) [9-16]. This is explained by the fact that according to the binary Nb-N phase diagram, the δ-NbN phase with a high T_c [17] does not form at temperatures below 1300 °C [18]. However, heating a cavity to such temperatures is not favorable because its mechanical properties and geometry would severely suffer [19]. Thus, nitriding processes at temperatures below 1000 °C are of great interest for SRF applications. Few papers describing such treatments are found in the literature. In reference [8], material with T_c=11.5 K after 800 °C annealing of niobium (evidently, fine-grain Nb) with 0.01 mbar of nitrogen for 5 min was obtained. A cavity oscillating at 9 GHz in a TE011 mode treated in a same way showed surface resistance of $2.8 \cdot 10^{-5}$ Ohm at 5.5 K, comparable to that of sputtered NbN, and a relatively low energy gap ($\Delta(0)=1.4\ k_B T_c$). It was assumed that the latter parameter was affected by $NbN_{0.8}O_{0.2}$ formation; however, no structural characterization was presented in this work. In another recent study, the structural, electronic and mechanical properties of large-grain niobium nitrided at 900 °C using 1.33 mbar of N_2 and differing nitriding durations (5 to 80 min) were investigated [16]. The nitride stoichiometry was determined to be hexagonal β-Nb_2N with N/Nb of 0.67-0.74 and mean crystallite size of ~18 nm. X-ray photoelectron spectroscopy (XPS) studies revealed strong oxygen contamination during and/or after such treatment; multiple peak fitting indicated NbN_xO_y and Nb_2O_5 formation.

Given this relative lack of data, a detailed study of the niobium surface treated at low partial pressures of nitrogen and moderate temperatures (below 1000 °C) is interesting both from the fundamental point of view and for SRF applications in accelerators. We have investigated Nb(100) single crystal surfaces prepared by buffered chemical polishing of large-grain cavity-grade Nb nitrided up to 900 °C. This paper reports on how the surface properties of Nb change after nitridation, investigated by means of scanning electron microscopy (SEM) in planar view and on focused ion-beam (FIB) prepared cross-sections, atomic-force microscopy (AFM), energy-dispersive X-ray analysis (EDX), glow-discharge optical-emission spectroscopy (GDOES), X-ray diffraction (XRD), and X-ray photoelectron spectroscopy (XPS).

Materials and methods:

The niobium discs (10 mm diameter, 2.8 mm height) with (100) crystal orientation were cut by electrical-discharge machining from the large-grain Nb ingots delivered by the Hereaus company. The sample preparation included treatment in a buffered chemical solution

($HF:HNO_3:H_3PO_4$ =1:1:2) to remove several tens of micrometers from the surface, followed by thorough washing in flowing water and an ultrasonic bath with ethanol.

The vacuum furnace used for the treatment of Nb in a nitrogen atmosphere consisted of a ceramic tubular chamber (diameter 70 mm, 1500 mm length) operating at a maximal temperature of 1200 °C and at a base pressure of 5×10^{-6} and 7.8×10^{-6} mbar at 800°C and 900°C, respectively, which are the temperatures of nitridation. Before nitridation, the samples were outgassed for two hours in vacuum at the corresponding temperature of nitridation. The attained background pressure value was equal to the process vacuum pressure for the thermal treatment of EXFEL cavities, according to the corresponding technical specification [20]. The nitrogen was supplied at a partial pressure of 0.04 mbar (30 mTorr) in a constant flow mode during the experiment. After 20 min, the nitrogen supply was terminated while the temperature was maintained constant for additional 30 min. The power supply was subsequently switched off and the samples were left in vacuum to cool down to room temperature.

The surface topography of the samples was studied using a 3D Laser Scanning Microscope. It utilizes a pinhole confocal optical system with a halogen lamp as a light source for optical or a red semiconductor laser for laser observation. The surface morphology was examined by SEM equipped with an EDX detector with a 150 mm² active area [21]. EDX spectra were performed with an acceleration voltage of the incident electron beam of 5 kV. The elemental depth profiles of the treated Nb samples were investigated by GDOES in OFG-Analytic GmbH (München, Germany). The detection limit for N, O, F was 220, 150, 185 wt. ppm respectively, which corresponds to 0.146, 0.087 and 0.090 as a % in pure Nb. The focused ion-beam cross-sections were prepared with a dual-beam FIB/SEM instrument with a final milling using a voltage for the Ga ions of 30 kV and an ion current of 0.3 nA. Before the cross-section preparation, a protective layer was deposited by ion-beam-induced deposition (IBID) using a precursor material containing platinum. AFM in tapping mode was used to map the surface topography of the sample annealed at 900 °C. Elemental and phase analyses were performed by X-ray Photoelectron Spectroscopy using a high-resolution 2D delay-line detector. A monochromatic Al K_α X-ray source (photon energy 1486.6 eV; anode operating at 15 kV) was used to provide incident radiation. The XPS spectra were recorded in fixed transmission mode. A pass energy of 25 eV was chosen, resulting in an overall energy resolution of better than 0.4 eV. X-Ray diffraction experiments were conducted to determine the phase composition of the samples as well as their epitaxial relation with the substrate. For this purpose, a six-circle diffractometer [21] with Cu K_α source was employed in both specular and grazing incidence geometries [22, 23]. Extensive reciprocal space maps in the $(h\ 0\ l)$ plane were performed with a fixed incident angle of 1.3° and

different exit angles, corresponding to a scattering depth in the range 100 nm - 200 nm for pure Nb for Cu K_α radiation [24]. The Bragg reflections were indexed by comparing the extracted adjacent lattice-plane distance, *d,* from the data with the existing ICSD database for powder diffraction. Here, the notation $(h\,k\,l)$ for bulk Nb coordinates was used, where its lattice parameters are $a = b = c = 3.303$ Å and $\alpha = \beta = \gamma = 90°$.

Results

GDOES

The concentration depth profiles of the treated samples were analyzed by GDOES. The concentration values of impurities in the nitrided Nb drop to the detection limit of the equipment within the first few micrometers (**Fig.1)**. Along with Nb, O and N elements, trace amounts of F were detected in all the samples (not shown), which originates from the fluoric acid used during sample preparation. The uncertainty of the actual depth profile obtained by GDOES is relatively high and therefore these results must be interpreted with care. Nevertheless, they do provide insight into the presence of N and can be correlated with the other techniques used in this study. In the end, the GDOES results can be used to estimate an upper limit for the penetration depth of N into the Nb.

According to the binary Nb-N phase diagram [17] the solubility of nitrogen in Nb at 800-900 °C is very low, i.e. the nitride phases immediately precipitate on its surface. Taking the experimental data of Albrecht and Goode [25], the terminal solubility of nitrogen in niobium would be 0.29 at% and 0.5 at% for the nitridation at 800 °C and 900 °C, respectively. In **Fig. 1**, the corresponding terminal solubility values for nitrogen in Nb are marked as horizontal dashed lines $C^N_{term\,800\,°C}$ and $C^N_{term\,900\,°C}$. Below these concentrations, nitrogen atoms are most likely located in interstitial positions of bcc Nb lattice (in α-NbN_x phase). Thus, the thickness of the formed nitrides would be about 3 µm for nitridation at 800 °C and 900 °C. It is noteworthy that the counts in the GDOES measurement spectra decrease sharply below these concentration values, which are close to the GDOES detection limit (0,087 at% N). A sharp drop of nitrogen concentration at the boundary of the nitride phase with the solid solution is normally observed. Oxides are also present, which form during the initial outgassing at the nitridation temperature at elevated residual pressures in the 10^{-6}-10^{-5} mbar regime, which are too high to keep the reactive Nb surface clean.

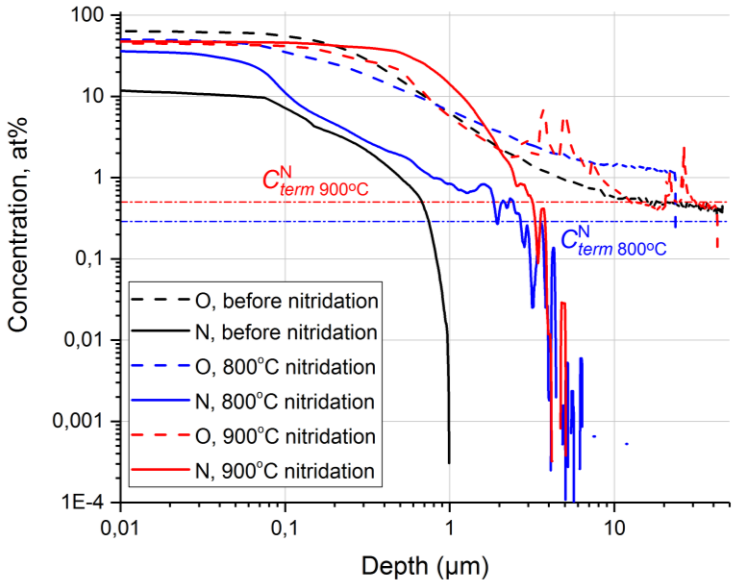

Fig. 1 Nitrogen and oxygen concentration profiles measured by GDOES. Horizontal lines represent the terminal solubility values of nitrogen C^N_{term} in pure Nb at 800°C and 900°C, respectively [25].

Optical Microscopy

The topological changes of the Nb surface observed by a laser microscope upon nitrogen thermal treatments are presented in **Fig. 2**. The typical etching features for a (100)-oriented Nb surface after BCP are seen [26]**. Figures 2(a)** and **2(b)** correspond to the same area before and after 800 °C nitridation, respectively. On the treated sample, randomly distributed tiny precipitates of triangular shape are observed. As shown in **Fig. 2(c)**, the surface topography of the sample treated at higher temperature has changed significantly, because the precipitates completely cover the sample surface. The average roughness parameters of the samples before and after nitridation measured over an area of 25 µm^2 are presented in **Table 1**. Generally, the mean roughness increases as the temperature of nitridation increases. However, for the 800 °C-treated sample, the average peak height R_p (**Table 1**) is the largest, which is caused by the formation of the large triangular-shaped precipitates.

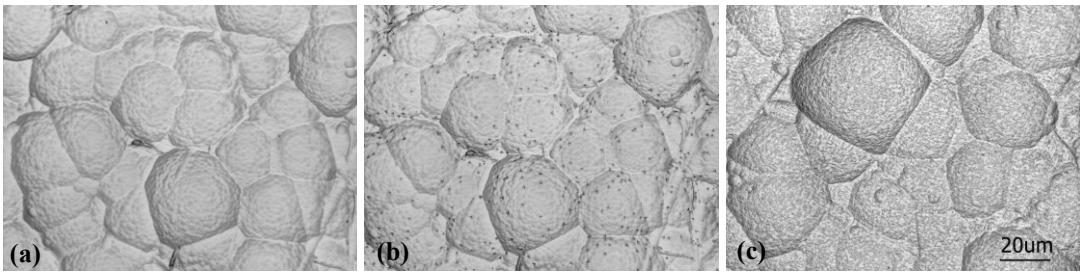

Fig. 2. The surface topography observed by a laser scanning microscope: (a) the initial Nb sample, (b) after nitridation at 800 °C and (c) 900 °C. The scale bar is valid for all figures.

Table 1. Average roughness parameters in an area of 25 μm^2, averaged over 10 different locations of the Nb samples nitrided at different temperatures. (R_a – arithmatic average, R_q – root-mean-square value, R_p – average peak height, R_v – average valley depth.)

	R_a (µm)	R_q (µm)	R_p (µm)	R_v (µm)
Initial	0.009	0.012	0.036	0.045
800 °C	0.027	0.035	0.218	0.139
900 °C,	0.037	0.047	0.154	0.179

Field-Emission Scanning Electron Microscopy, EDX and FIB based cross-section imaging:

The topographical contrast images obtained with a secondary electron detector on the nitrogen-treated samples are presented in **Fig. 3**. After the 800 °C nitrogen treatment, a few 1-2 µm micrometer triangular precipitates of a new phase clearly appear on the sample surface (**Fig.3a**) with density of 3.2 precipitates per 100 μm^2, while at higher magnification (**Fig.3b**), approximately 20 × (50−100) nm^2 rectangular-shaped precipitates with density of ~ 25 precipitates per 1 μm^2 can be observed. The different geometry of these two precipitates indicates that the type of crystal lattice is different, and therefore it can be assumed that the phase composition of these precipitates is also different. The EDX map (**inset of Fig. 3a**) visualizes the elemental distribution of Nitrogen over the sample surface, indicating that the triangular precipitates are nitrogen enriched. From the EDX elemental point analysis, the nitrogen (oxygen) content was found to be ~35(2) at % and ~2(8) at % at the center of the triangular precipitates and the surrounding area, respectively (see **Table 2**).

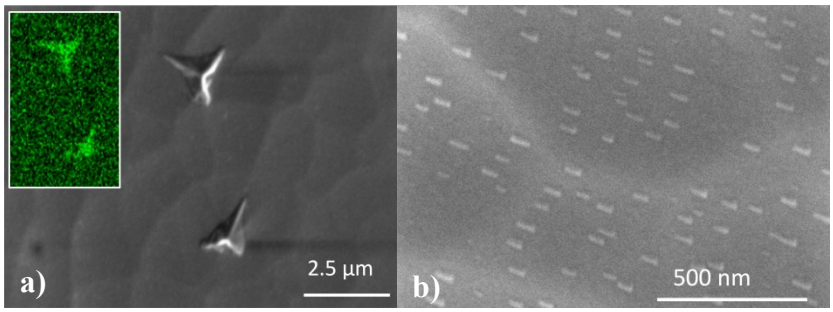

Fig. 3. Scanning electron micrographs of Nb samples nitrided at 800 °C, (inset in a: EDX elemental map for N K_α).

After the 900 °C nitrogen treatment, the surface topography underwent significant changes compared to at 800 °C. The rectangular-type precipitates have larger dimensions (60-100 nm in width, up to ~250 nm in length) and are distributed much more densely (**Fig. 4 a**), thus forming a layer of closely packed precipitates. The EDX revealed increased nitrogen content upon such treatment, while the oxygen content remained at approximately the same level (**Table 2**). Carbon was omitted from the analysis, since its presence seems to be overestimated due to accumulation of carbon species on the sample surface during the measurements of EDX spectra.

Table 2: Elemental composition in atomic percent obtained from EDX point measurements for different samples. For the 800 °C sample, the values are given for a point 'A' in the area containing triangular precipitates, and another point 'B' in the area surrounding triangular precipitates shown at higher resolution in Fig.3b.

Element	**Initial**	**800 °C**		**900 °C**
		A	**B**	
N	-	35.69	2.41	40.88
O	7.51	2.25	7.82	3.08
Nb	92.49	62.06	89.78	56.04
Total	100.00	100.00	100.00	100.00

A typical topographic scan measured by means of AFM on the 900 °C nitride Nb is given in **Fig. 4 (b),** and a height profile in **Fig. 4 (c),** along a line drawn almost perpendicular to the rectangular precipitates. This shows that the rectangular islands are approx. 13 nm high and 75 nm wide, in agreement with the SEM observations on the same sample.

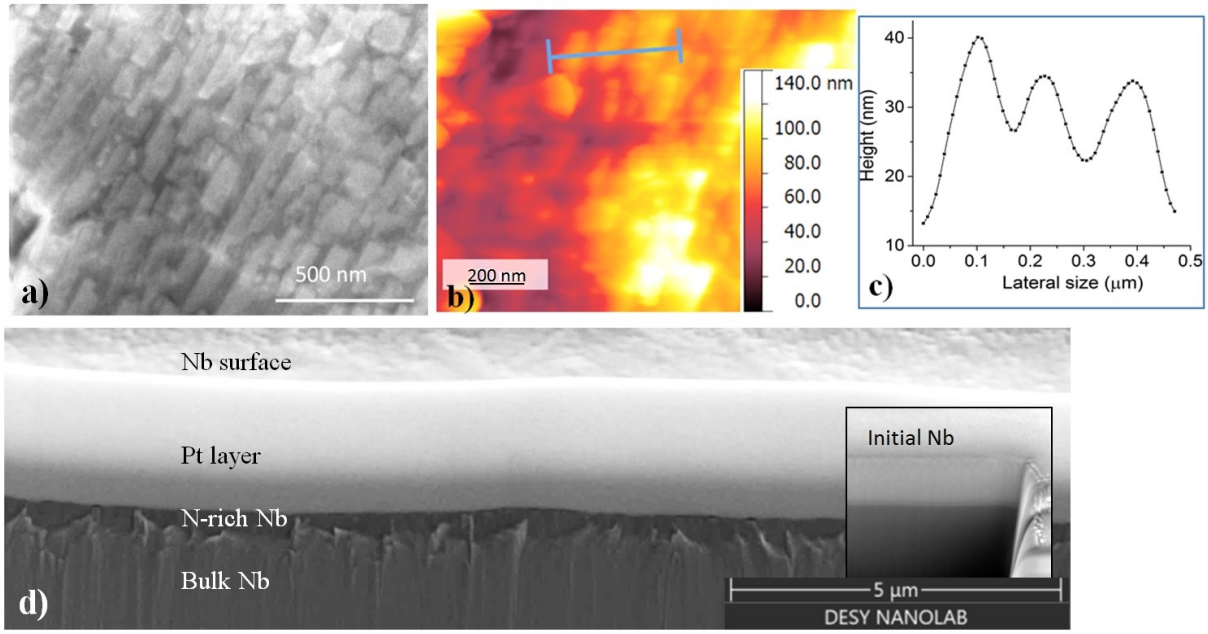

Fig. 4. (a) SEM and (b) AFM surface topography of the Nb sample after nitride treatment at 900 °C; (c) the corresponding AFM height profile along the 0.5 µm line drawn in (b); (d) SEM image of the FIB-prepared cross section of the 900 °C sample with the initial Nb sample in the inset.

Fig. 4(d) shows an SEM section view of a FIB prepared ~ 5 µm deep cross section of the 900 °C nitrided sample. A corrugated layer between the uppermost Pt-based protection layer and the underlying bulk can be observed, which appears dark and extends over a depth of approximately 400 nm. This indicates that the large concentration of nitrogen deduced by GDOES in the near surface region leads to a local mechanical hardening that could induce a different milling behavior and obstruct the creation of a smooth bulk cross-section surface underneath. Since this dark region is absent from the initial sample, as can be seen in the inset in Fig. 4d, this clearly shows that the origin of the corrugated layer is due to the nitridation at 900 °C.

X-ray diffraction:

Crystallographic information of the 900 °C nitride sample was retrieved from specular and in-plane X-ray diffraction measurements. **Fig. 5(a)** shows the specular diffraction profile, where the presence of two different phases, cubic NbO (space group *Fm-3m*) and hexagonal β-Nb_2N (space group *P63/mmc*) was observed. The Bragg reflections were indexed as (200) NbO ($2\theta = 42.70°$) and ($\bar{1}02$) β-Nb_2N ($2\theta = 50.55°$), according to the Inorganic Crystal Structure Database (ICSD) collection codes 61543 for NbO, and 76387 for β-Nb_2N. The reflections at 38.45° and 55.66° were assigned to (110) and (200) of bulk Nb.

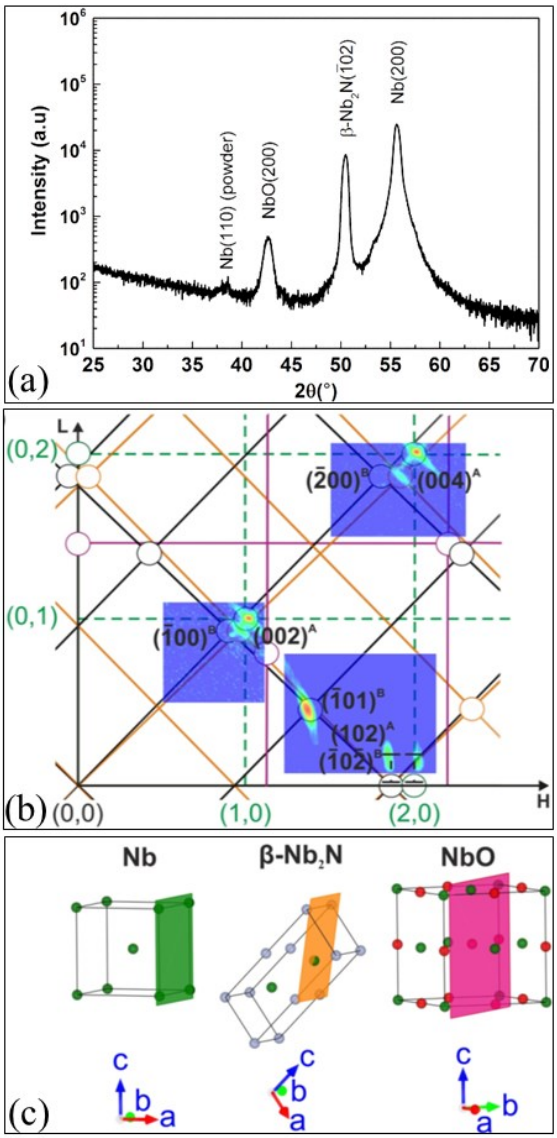

Fig 5(a). Specular diffraction profile of the 900 °C treated sample. The observed Bragg peaks can be indexed using β-Nb_2N, NbO and bulk Nb phases. (b) Reciprocal-space maps in selected areas and the corresponding reciprocal lattice of Nb (green), β-Nb_2N (orange/black) and NbO (magenta) assuming a particular epitaxial orientation and two domains for the nitride: A (orange) and B (black). Open circles represent expected intensities in reciprocal space. (c) Real-space model of Nb, β-Nb_2N and NbO, with N atoms depicted in grey and O atoms depicted in red. For all real space models, dark green atoms represent Nb atoms. See text for details.

The absence of other reflections corresponding to NbO and β-Nb_2N in the out-of-plane direction suggest neither a powder-like nor a textured growth but rather an epitaxial growth of these phases on the surface of the large-grain Nb. β-Nb_2N is known to be formed with heat treatments above 500 °C in the presence of nitrogen [27]. However, the majority of the works reported in literature show polycrystalline diffraction features for this phase, even for large-grain Nb substrates [16], in contrast to that proposed in this work. As reported in [16], the thermal

treatment of large-grain and single-crystalline Nb with 1.33 mbar N_2 pressure at 900 °C leads to the formation of single-phase polycrystalline β-Nb_2N with reaction time as low as 5 minutes. Recently, the presence of β-Nb_2N in fine-grain Nb samples cut out from cavities treated at 800 °C with 0.02 mbar for reaction times varying between 2 and 20 minutes was confirmed [7]. Similar to the results presented in this paper, the nitride precipitates showed particular epitaxial orientation related to the substrate observed through nano electron diffraction patterns in selected areas within the fine grains.

Epitaxial growth of NbO was observed with a different Nb crystal orientation, namely (110). The formation of epitaxial (111)-oriented NbO in oxidized Nb(110) thin films was reported in [28], while for Nb(110) surfaces annealed in UHV above 900°C, a NbO overlayer is created, presenting a Kurdjumov-Sachs epitaxial relationship [29]. Epitaxial (111)-oriented NbO was also observed for single-crystalline Nb(110) after heating at 300 °C under UHV conditions [30].

The in-plane structure and epitaxial relationship between NbO, β-Nb_2N and the Nb substrate summarized in **Table 3** were obtained by collecting extensive reciprocal-space maps with a fixed incidence angle of 1.3°, corresponding to a scattering depth between 100 nm to 200 nm. **Fig. 5(b)** shows the maps collected at the plane $k = 0$ of Nb with the sketch of the corresponding reciprocal lattices. The presence of two different domains of β-Nb_2N was observed, mentioned hereafter as domain A (orange grid in Fig. 5(b)) having the (002) and (004) reflections in the vicinities of (101) and (202) reflections of the Nb lattice. Domain B (black grid in Fig. 5(b)) has its lattice rotated 180° around the (002) Nb reciprocal lattice vector and therefore with the $(\bar{1}0\bar{1})$ reflection sitting at the $k = 0$ plane of Nb. Effects arising from crystal miscut and strain of the formed phases should be taken into account to give a precise match between the calculated positions of the reciprocal-space intensities and the actual measured data. Here, the c/a ratio of the β-Nb_2N grains was calculated to be 1.678, with $a = 2.945$ Å and $c = 4.941$ Å, corresponding to a difference of about 3.43% when compared with the standard value of 1.622 (ICSD 76387). Reflections belonging to NbO (hhl) plane, which here coincides with the $(h0l)$ plane of Nb, were not seen in the collected reciprocal space maps but were measured with an omega scan taken with the detector fixed at the (111) NbO Bragg position while the sample was rotated around the surface normal (**Fig. S1**). The expected intensity positions of NbO (111) and (222) Bragg peaks are also shown in the reciprocal lattice sketch of **Fig. 5(b)**.

Table 3. Epitaxial relation between the different phases identified by GIXRD and the Nb substrate in the 900°C treated sample. The superscripts A and B indicate the two different nitride domains present. See text for details.

Phase	Epitaxial Relation with respect to Nb
NbO	$(100) \parallel (110)$
	$(001) \parallel (001)$
β-$Nb_2N^{A,B}$	$(\bar{1}02)^{A} \parallel (001)$
	$(102)^{A} \parallel (100)$
	$(\bar{1}02)^{B} \parallel (001)$
	$(\bar{1}0\bar{2})^{B} \parallel (100)$

Combining the specular and reciprocal space mapping information gives the real space models of both β-Nb_2N and NbO with respect to Nb, as shown in **Fig. 5(c)**. For β-Nb_2N, the (102) plane - depicted in orange - is parallel with respect to the (100) plane of Nb, showed in green. For NbO the magenta plane represents the (110) index, which is parallel to the (100) plane of Nb, meaning that the NbO lattice is rotated 45° around the surface normal with respect to the substrate, sharing the same (002) out-of-plane orientation.

XPS:

The XPS measurements were performed on the initial and nitrogen-treated (at 800 °C and 900 °C) Nb samples after air exposure. For all spectra, the binding energies were calibrated based on the Nb 3d peak at 207.6 eV assigned to Nb_2O_5, which is known to form the uppermost surface layer on NbN after its oxidation in air [31]. The area ratio for the Nb 3d spin-orbit doublets was fixed to 1: 0.67 with an energy difference of 2.7 eV. The XPS survey spectra (or an overview of the Nb 3d, N 1s, O 1s and C 1s line shapes - given in the supporting material (**Fig. S2**) mainly shows an increased N 1s peak intensity and suppressed Nb 3d peak intensity for the niobium nitrided at higher temperature, suggesting higher nitride coverage of the surface. This is in-line with the microscopic investigation, which revealed the presence of a 400 nm thick surface layer in FIB cross-sectional image for the 900 °C nitrogen treated Nb and approximately 10 nm thin uniform layer of densely-packed rectangular precipitates. For the same reason, the metallic Nb peak (~202 eV) is no longer observable in the XPS spectra of this sample. No appreciable changes in the O 1s and C1s lines are seen for the Nb before and after the nitrogen treatment. In all cases, the O 1s spectra contain the most intense peak corresponding to the Nb_2O_5, while the C 1s spectra show mainly the presence of C-C, and C-O bonds. In the C 1s core-level spectra, no peak is

observed in the range of 282 eV- 283 eV - corresponding to the binding energy of a Nb-C bond [32, 33]; therefore, the presence of NbC phase can be ruled out in all of the investigated samples.

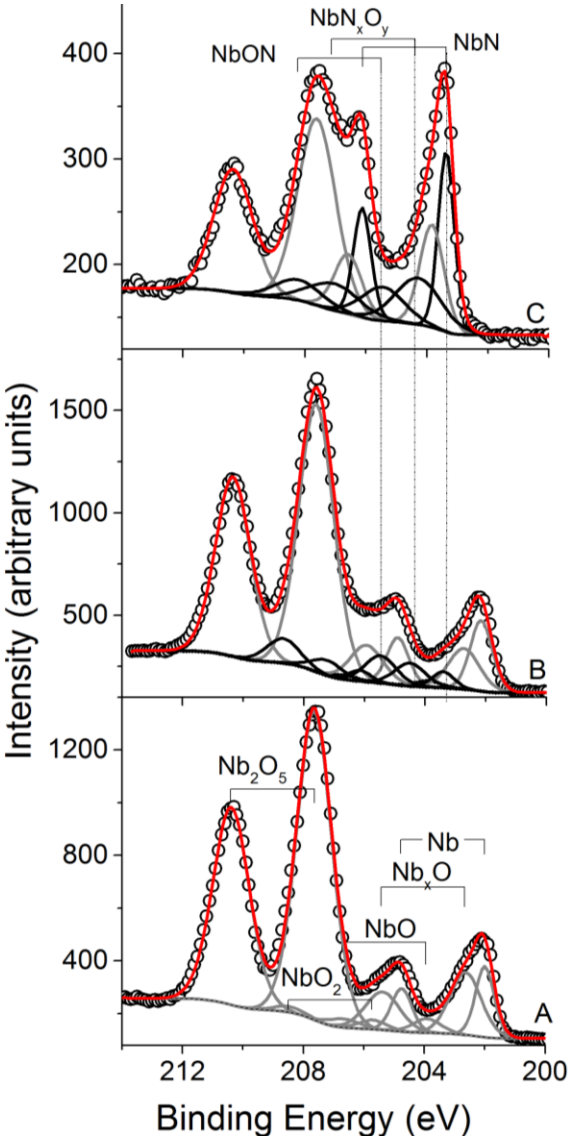

Fig. 6. Deconvoluted Nb 3d lines measured for the Nb samples in initial stage (A), and after nitridation at 800 °C (B) and 900 °C (C). The grey fit lines indicate the phases corresponding to the Nb and Nb oxides, while the black fit lines represent the Nb nitrides/oxynitrides.

Fig. 6 and **Fig. 7** show the deconvolution of XPS spectra of Nb 3d, and N 1s in Nb measured at room temperature for the initial and after nitrogen treatment at 800 °C and 900 °C, respectively. The Nb 3d region of the initial niobium consists of a number of doublets with binding energies in a descending order for Nb $3d_{5/2}$ at 207.6, 205.7, 203.9, 202.6 and 202.0 eV,

which are assigned to Nb_2O_5, NbO_2, NbO, Nb_xO , and metallic Nb components, respectively. These values are in a very good agreement with the literature [31], which reports on UHV-annealed Nb [30] and buffered chemically polished Nb [2] after a long oxidation in air. Here, Nb_xO may contain the components from Nb_2O and other niobium oxides, indicating a gradual transition of the structure within different bulk densities, which helps to release the strain in the material. After nitrogen treatment, the formation of niobium nitride is confirmed by XRD. However, the overlapping of the corresponding peaks with those for the oxides of niobium makes the deconvolution of Nb 3d line difficult. A comparison of the results obtained from the deconvolution of Nb 3d (**Fig. 6)**, N 1s (**Fig. 7**), O 1s and C 1s lines (**Fig. S3**) all together help to clarify the present components, resulting in the labelling of the retrieved phases in the corresponding figures.

For the 800 °C nitrided Nb sample, pure Nb is revealed by XPS since the surface is only partially covered by niobium nitride and oxides. A shift of the Nb 3d binding energies to higher values compared to the initial Nb sample has been observed, which suggests a change in the chemical composition. The metallic Nb peak shifts from 202.0 eV in initial sample to 202.2 eV in 800 °C annealed sample, indicating the presence of small amount of NbN, which is in line with the occurrence of a broad N1s peak in the range of 396 - 397 eV - corresponding to the N bound to Nb in niobium nitride and oxynitrides.

For 900 °C nitrided Nb, the Nb 3d peaks change substantially and show a large decrease of Nb_2O_5 oxide peaks centered at 207.6 ($Nb3d_{5/2}$) and 210.3 eV ($Nb3d_{3/2}$), while the NbO peaks at 203.8 eV ($Nb3d_{5/2}$) and 206.6 eV ($Nb3d_{3/2}$) increase in intensity, showing a reduction of Nb cations under nitrogen atmosphere at elevated temperatures. Besides Nb_2O_5 and NbO components, the newly emerged Nb 3d peaks at binding energies 203.4 eV, 204.3 eV and 205.5 eV are observed, which are attributed to the NbN, NbN_xO_y and NbON phases, respectively. It is known that intermediate non-stoichiometric phases of NbN_xO_y are formed as a transition between the NbN and Nb_2O_5 due to the oxidation process [31].

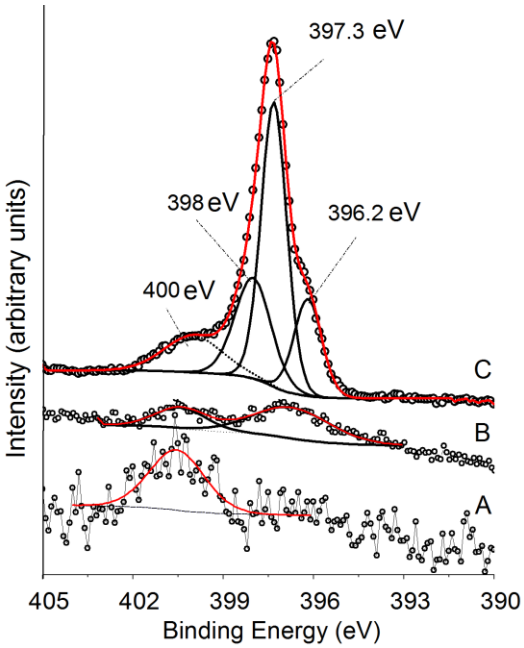

Fig. 7. Deconvolution of N 1s lines measured for the Nb samples in initial stage (A), and after nitridation at 800 °C (B) and 900 °C (C).

For the 900 °C treated sample, the N 1s peak at 397.3 eV increased greatly in intensity, showing the huge nitritation of Nb as proved by the Nb 3d peak at 203.3 eV; a lower-energy peak at 396.2 eV was assigned to NbON, in line with the Nb 3d peak at 205.5 eV. This is in agreement with that reported in ref. [31] for a ~10 nm thick superconducting NbN surface layer on Nb. A higher binding-energy peak at ~400 eV is observed in all cases including the initial Nb, which is due to the adsorbed nitrogen on the surface [34, 35]. Moreover, another N 1s peak observed at 398 eV is attributed to the β-Nb_2N phase. The presence of hexagonal β-Nb_2N phase was also confirmed by the X-ray diffraction; however, the δ-NbN could not be detected most probably because of the Bragg peaks overlapping with that for NbO (lattice parameter 4.38 Å for the former and 4.21 Å for the later) or very low amount of the material present. A recent study on niobium nitride thin films shows that the N 1s core levels for cubic fcc (δ-NbN) and hexagonal (β- Nb_2N) structures are located at 397.2 eV and 397.9 eV, respectively [36]. There it was also deduced that the latter had a higher covalent-bonding character and the valence-band energy-distribution curves were significantly different in both cases. The present photoelectron measurements hint at the presence of a δ-NbN component on the surface of nitrogen-treated Nb at 900 °C; however, more detailed investigations, e.g. a systematic depth-profiling XPS and X-ray diffraction in a wider angular range are needed to gain more insight on the sub-surface compositions of the samples.

Discussion:

After 900 °C nitridation of Nb (100), a uniformly dense layer of epitaxial rectangular precipitates is observed on the surface and a corrugated layer of 400 nm is seen in FIB cross-sectional image. GDOES results show that the nitrogen-enriched region lies within a depth of ~3 μm from the surface; while the phases of NbO and β-Nb_2N were identified by means of X-ray diffraction in the top ~200 nm of the material. XPS indicates the presence of Nb_2O_5, NbO, β-Nb_2N, δ –NbN, NbN_xO_y and NbON in the top ~5 nm surface region. On 800 °C nitrided Nb, triangular precipitates grow in addition to rectangular ones. They are sparsely decorated and are nitrogen rich, containing the hexagonal β-Nb_2N phase, analogous to that reported in reference [7]. Moreover, XPS data confirms the presence of a non-stoichiometric phase of NbN_xO_y and NbON, which is in a good agreement with the observations on air-oxidized niobium nitride [31]. The presence of β-Nb_2N on the cavity surface has been found to be detrimental to their performance and therefore the top surface material must be removed up to an optimum depth in the micron range [5, 8].

Even though the phases identified above are present in the top 200 nm near-surface region, the impact of nitridation still remains after removal of a few μm of the upper surface layer. Most probably, the interstitial N, C or O content within the Nb near-surface region is affected by nitridation in such a way that their concentration and distribution is optimum, leading to an enhanced cavity performance. It is already known that the presence of N-interstitials at octahedral sites functions as an effective trap for hydrogen at tetrahedral sites in the Nb lattice [37, 38]. This prevents the formation of niobium hydrides on the cavity surface during the cool-down phase and thus gets rid of the corresponding Q-degradation in the cavities. Moreover, the density of impurities/interstitials at the cavity surface affects the mean free path of electrons, which further influences the surface resistance of Nb [39]. For example, existence of a minimum in the surface resistance of a Nb cavity has been observed after a 120 °C bake for 48 hours, which is a well-established step in cavity processing to boost the SRF performance [40]. In another study, a decreased mean free path was observed after each low temperature bake at 120°C for 12- 24 hours of a large-grain Nb cavity following a high temperature annealing for few hours in 800 °C- 1400 °C range [41]. An exceptionally high Q value was achieved after a 1400 °C annealing step which resulted in Ti doping of Nb from the cavity flange, as confirmed by the elemental analysis of corresponding Nb samples exhibiting an increased concentration of Ti, C, N, and O together with the significantly reduced H content in the near surface region [41]. Since different annealing

cycles can redistribute the impurities at the cavity surface [3], a certain impurity distribution at the Nb surface can lead to a minimum in the surface resistance, and thus might result in an enhanced cavity performance [39, 41]. Therefore, it becomes important to study the interstitial distribution in the near-surface region of Nb by suitable methods, for example by diffuse X-ray scattering.

Conclusions:

The influence of nitrogen thermal treatment at 800 °C and 900 °C on the surface of large grain Nb(100) samples made up of SRF-cavity-grade Nb and the surface prepared by the standard cavity processing step of buffered chemical polishing has been investigated. On Nb nitrided at higher temperature, GDOES shows an excess of nitrogen at a depth of about a few μm from the surface. Under this condition, the surface was completely covered by a thick dense layer of more than 10 nm high epitaxial rectangular precipitates; a corrugated surface layer of thickness less than half a micrometer was observed by SEM on a FIB-prepared cross-section. Crystallographic phases of NbO and β-Nb_2N were identified by means of grazing-incidence X-ray diffraction. These agree with the results obtained by photoelectron spectroscopy measurements but in addition disclose the presence of NbON and NbN_xO_y components and the cubic phase of NbN in close vicinity to the surface within the XPS, probing depths of a few nm. Since these phases are no longer present in the cavities which undergo a final polishing step after the nitridation, the distribution of N interstitials in the near- surface region must be influenced be the nitridation process, which plays a key role in enhancing the cavity performance. It can however not be excluded that Nb oxide and interstitial oxygen, which are always present because of the moderate vacuum conditions during annealing, are not involved in the process. It is expected that future experiments employing much more controlled Nb-annealing conditions will deliver further insight into the observed cavity-performance improvement.

Acknowledgments

Authors declare that no conflicts of interest exist. Support on the material from Xenia Singer, and for the FIB preparation and the SEM analysis by S. Kulkarni at the DESY NanoLab, is acknowledged. We acknowledge the use of the focused-ion-beam instrument at the DESY NanoLab funded by the BMBF grant no. 5K13WC3 (PT-DESY). Authors GSD, AP and BF acknowledge funding from the BMBF grant no. 05H15GURBB.

[1] Ciovati G, Kneisel P and Gurevich (2007) A Measurement of the high-field Q drop in a high-purity large-grain niobium cavity for different oxidation processes, Phys Rev ST Accel. Beams 10, 062002.

[2] Ma Q and Rosenberg RA (2003) Angle-resolved X-ray photoelectron spectroscopy study of the oxides on Nb surfaces for superconducting rf cavity applications, Appl Sur Sc 206:209-217.

[3] Ciovati G, Myneni G, Stevie F, Maheshwari P and Griffis D (2010) High field Q slope and the baking effect: Review of recent experimental results and new data on Nb heat treatments, Phys Rev Accel Beams 13:02200.

[4] Grassellino A, Romanenko A, Trenikhina Y, Checchin M, Martinello M, Melnychuk O S, Chandrasekaran S, Sergatskov D A, Posen S, Crawford A C, Aderhold S and Bice D (2017) Unprecedented quality factors at accelerating gradients up to 45 MV/m in niobium superconducting resonators via low temperature nitrogen infusion, Supercond Sci Technol 30:094004.

[5] Grassellino A, Romanenko A, Sergatskov D, Melnychuk O, Trenikhina Y, Crawford A, Rowe A, Wong M, Khabiboulline T and Barkov F (2013) Nitrogen and argon doping of niobium for superconducting radio frequency cavities: a pathway to highly efficient accelerating structures, Supercond Sci Technol 26:102001.

[6] Grassellino A, Romanenko A, Posen S, Trenikhina Y, Melnychuk O, Sergatskov D A, Merio M, Checchin M, Martinello M (2015) N doping: progress in development and understanding. Proc SRF2015, Whistler, BC, Canada, MOBA06, pp 48-754 (2015).

[7] Trenikhina Y, Grassellino A, Barkov F and Romanenko (2013) A chemical structure of niobium samples vacuum treated in nitrogen in parallel with very high Q_0 cavities, Proc SRF2013, Paris, France, TUP065, pp 583-585.

[8] Trenikhina Y, Grassellino A, Melnychuk O and Romanenko A (2015) Characterization of nitrogen doping recipes for the Nb SRF cavities. Proc SRF2015, Whistler, BC, Canada, MOPB055, pp 223-227.

[9] Pham Tu M, Mbaye K, Wartski L and Halbritter J (1988) RF characterization of thermally diffused superconducting niobium nitride, J Appl Phys 63:4586-4590.

[10] Fabbricatore P, Fernandes P, Gualco G, Merlo F, Musenich R and Parodi R (1989) Study of niobium nitrides for superconducting rf cavities, J Appl Phys 66:5944-5949.

[11] Benvenuti C, Chiggiato P, Parrini L and Russo R (1993) Reactive diffusion produced niobium nitride films for superconducting cavity applications, Nuc Instr Meth Phys Res A: Accelerators, Spectrometers, Detectors and Associated Equipment 336:16-22.

[12] Fabbricatore P, Gemme G, Musenich R, Parodi R, Viviani M, Zhang B and Buscaglia V (1993) Niobium and niobium-titanium nitrides for RF applications, IEEE Trans on Appl Superc 3:1761-1764.

[13] Joguet M, Lengauer W, Bohn M and Bauer J (1998) High-temperature reactive phase formation in the Nb-N system, J Allo and Comp 269:233-237.

[14] Lengauer W, Bohn M, Wollein B and Lisak K (2000) Phase reactions in the Nb–N system below 1400° C, Act Mat 48:2633-2638.

[15] Linde A, Marin-Ayral R-M, Granier D, Bosc-Rouessac F and Grachev V (2009) Synthesis of cubic niobium nitride by reactive diffusion under nitrogen pressure, Mat Res Bull 44:1025-1030.

[16] Ufuktepe Y, Farha AH, Kimura S-i, et al. (2013) Structural, electronic, and mechanical properties of niobium nitride prepared by thermal diffusion in nitrogen, Mats Chem Phys 141:393-400.

[17] Vonsovsky SV, Izyumov YA and Kurmaev EZ (1982) Superconductivity of transition metals. Springer-Verlag Berlin Heidelberg, Germany

[18] Brauer G and Esselborn R (1961) Nitridphasen des Niobs, Zeits Anorg Allg Chem 309:151-170.

[19] отжиг резонатора – геометрия, мех свойства

[20] Series surface and acceptance test preparation of superconducting cavities for the European XFEL, Revision B/June 30, 2009, p. 22

[21] Deutsches Elektronen Synchrotron (DESY). (2016). DESY NanoLab. Journal of large-scale research facilities, 2, A76. http://dx.doi.org/10.17815/jlsrf-2-140.

[22] Lohmeier M and Vlieg E (1993) Angle calculations for a six-circle surface X-ray diffractometer, J Appl Cryst 26:706-716.

[23] Vlieg E (1997) Integrated intensities using a six-circle surface x-ray diffractometer, J Appl Cryst 30:532-543.

[24] Dosch H (1992) Critical phenomena at surfaces and interfaces - evanescent x-ray and neutron-scattering. Springer tracts in modern physics, 126:1.

[25] Albrecht WM and Goode Jr WD (1959) Reaction of nitrogen with niobium, Techn Rep BMI-1360, W-7405-ENG-92, Battelle Memorial Inst., Columbus, Ohio,13 p.

[26] Batchelor A, Leonard D, Russell P, Stevie F, Griffis D and Myneni G (2007) TEM and SIMS Analysis of (100),(110), and (111) Single Crystal Niobium. Conf Proc AIP, pp 72-83.

[27] Huang W (1996) Thermodynamic assessment of the Nb-N system, Metall and Mater Trans A 27:3591-3600.

[28] Matylitskaya V, Bock W and Kolbesen B (2008) Nitridation of niobium oxide films by rapid thermal processing, Anal Bioanal Chem 390:1507-1515.

[29] Arfaoui I, Cousty J and Safa H (2002) Tiling of a Nb (110) surface with NbO crystals nanosized by the NbO/Nb misfit, Phys Rev B 65:115413.

[30] Delheusy M, Stierle A, Kasper N, et al. (2008) X-ray investigation of subsurface interstitial oxygen at Nb/oxide interfaces, Appl Phys Lett 92:101911.

[31] Darlinski A and Halbritter J (1987) Angle-resolved XPS studies of oxides at NbN, NbC, and Nb surfaces, Surf Interface Anal 10:223-237.

[32] Ramqvist L, Hamrin K, Johansson G, Gelius U and Nordling C (1970) VC, NbC and TaC with varying carbon content studied by ESCA, J Phys Chem Sol 31:2669-2672.

[33] Nedfors N, Tengstrand O, Lewin E, Furlan A, Eklund P, Hultman L and Jansson U (2011) Structural, mechanical and electrical-contact properties of nanocrystalline-NbC/amorphous-C coatings deposited by magnetron sputtering, Surf Coat Technol 206:354-359.

[34] Havey KS, Jabinski JS, and Walck SD, The chemistry, structure, and resulting wear properties of magnetron-sputtered NbN thin films, Thin Solid Films 303, 238 (1997).

[35] Jouvey G, Severac C, and Cantacuzene S, XPS study of NbN and (NbTi)N superconducting coatings, Thin Solid Films 287, 146 (1996).

[36] Sanjinés R, Benkahoul M, Sandu C, Schmid P and Lévy F (2006) Electronic states and physical properties of hexagonal β-Nb2N and δ′-NbN nitrides, Thin Solid Films 494:190-195.

[37] Richter D, Töpler J and Springer T (1976) The Influence of Dissolved Nitrogen and Hydrogen in Niobium Studied by Neutron Spectroscopy, J. Phys. F: Metal. Phys. 6, 4.

[38] Metzger T H, Schubert U, and Peisel J (1985), The Trapping of Hydrogen at Nitrogen in Niobium Investigated by Diffuse X-ray Scattering, J Phys F: Metal Phys 15, 779.

[39] Gurevich A (2012) Superconducting radio-frequency fundamentals for particle accelerators, Rev Accel Sci Technol 5, 119-146.

[40] Ciovati G (2004) Effect of low-temperature baking on the radio-frequency properties of niobium superconducting cavities for particle accelerators, J App Phys 96, 1591.

[41] Dhakal P, Ciovati G, Myneni G R, Gray K E, Groll N, Maheshwari P, McRae D M, Pike R, Proslier T, Stevie F, Walsh R P, Yang Q and Zasadzinzki J (2013) Effect of high temperature heat treatments on the quality factor of a large-grain superconducting radio-frequency niobium cavity, Phys. Rev. ST Accel. Beams 16, 042001